Analysis of Antennas on Board Arbitrary Structures Modeled by Nurbs Surfaces

Jesús Pérez, *Student Member, IEEE*, Juan A. Saiz, *Student Member, IEEE*, Olga M. Conde, *Student Member, IEEE*, Rafael P. Torres, *Member, IEEE*, and Manuel F. Cátedra, *Member, IEEE*

***Abstract*—An accurate and efficient numerical scheme has been developed for predicting high-frequency radiation patterns of antennas mounted on arbitrary structures modeled by parametric surfaces. The method is based on geometric optics (GO) and the uniform theory of diffraction (UTD). Nonuniform rational B-splines (NURBS) surfaces have been used to describe the geometry of the structure. As most of the computer-aided geometric design (CAGD) tools available in the industry are based on NURBS, the scheme can perform the electromagnetic analysis without any new or additional remeshing of the geometrical model. A special ray-tracing technique that combines GO and UTD with NURBS has been developed. This technique uses some selective criteria in order to identify rapidly the NURBS where a ray impact may occur. Impact points coordinates are obtained by means of an optimization procedure based on the conjugate gradient method (CGM). The accuracy and efficiency of the approach are shown comparing it with other methods.**

***Index Terms*—Antennas, geometrical theory of diffraction.**

I. Introduction

THE solution of electromagnetic radiation problems of antennas on board arbitrary structures can be very cumbersome and computationally expensive. The main obstacle solving problems of this type using geometrical optics (GO) and uniform theory of diffraction (UTD) is that of achieving a realistic model with an affordable computational cost.

Previous studies of radiation patterns of airborne antennas were obtained modeling the different parts of the airplane using cylinders, ellipsoids, flat facets, and other canonical surfaces [1]–[6]. This type of description has a straightforward data structure based on a cross-referenced list of vertices, edges, and faces. However, when the structure under analysis is very complex, the modeling requires a very large number of canonic surfaces to describe accurately the real model. In this case, the CPU time and computer memory resources required are very large. The parametric surfaces were developed to replace these primitive representations in shipbuilding, automotive, and aircraft industries. Nonuniform rational B-spline (NURBS) description is able to manipulate free-form surfaces with a low number of patches and, therefore, with a low amount of information [7]. An example of an application of the NURBS form to a real model is shown in Fig. 1(a).

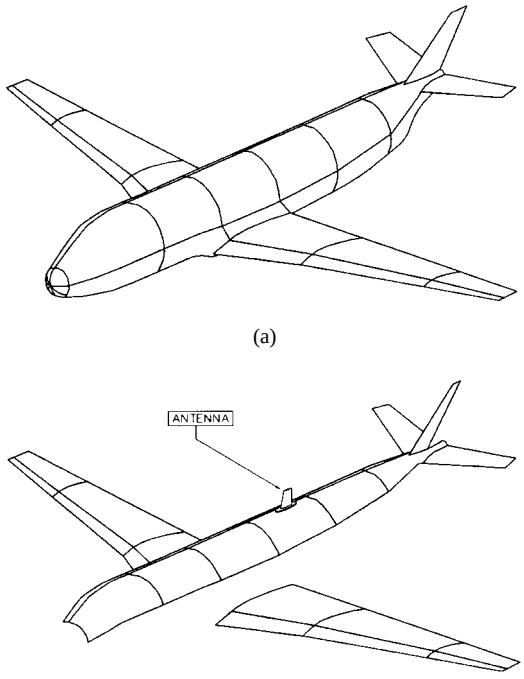

(a)

(b)

Fig. 1. (a) Example of an aircraft modeled by NURBS patches. (b) Selected Bèzier's patches (BP's) for the analysis of an antenna mounted on the top of the fuselage of the airplane.

From the authors' knowledge, attending to the open literature, NURBS were applied to computational electromagnetics, mainly in the area of radar cross-section (RCS) predictions [8]–[16]. In all these works, NURBS were employed for the modeling and storage of the targets. However, two different approaches were considered to compute the fields. In one approach [9], [13], [15], [16], the NURBS are used directly in the rendering processes. In addition, in this approach, the field values are computed by obtaining the geometrical data from the NURBS parameters. In the other approach [14], NURBS are used for modeling the object geometry, but subsequently, a graphical processing scheme is introduced to generate a pixel image of the target that is then used in a physical optics/physical theory of diffraction (PO/PTD) approximation to compute RCS values. The major advantage of this last approach is its efficient performance in the shadowing of the target when the method is directly implemented

Manuscript received January 22, 1996; revised November 15, 1996. This work was supported in part by CASA (Construcciones Aeronaúticas S.A.) and by the Spanish Advisory Commission for Scientific and Technological Research (CICYT), Projects Ref.TIC93-0671-C06-01 and TIC93-0671-C06-01.

The authors are with Grupo de Sistemas y Radio, Departamento de Ingeniería de Comunicaciones, Universidad de Cantabria, Santander, Cantabria, 39005 Spain.

Publisher Item Identifier S 0018-926X(97)04256-7.

using the software and hardware facilities available in the graphical treatment of most computers. The drawback of the method is that double interactions as double reflections and diffraction–reflection are quite difficult to treat with a pixel model.

Other works using NURBS in applied electromagnetics can be found in the moment method (MM), as in [17], where the basis and testing functions of a scheme were defined directly over these surfaces avoiding any additional remeshing.

Four main steps can be considered in the approach. The first step starts with the input of the geometry data in a NURBS format. After that, the NURBS surfaces are subsequently subdivided into a combination of rational Bèzier's patches (BP's) using the Cox-De Boor algorithm [18]. This transformation is applied because Bèzier format is more stable for the numerical rendering of each surface piece (interrogation about point coordinates, curvature radii, etc.), while NURBS are more efficient for the storage and representation of a complete model.

In the second step of the approach, one set of patches of the BP model is selected. This set of patches constitutes the BP's that presumably will contribute to the field levels. Only these selected patches (that we will call "illuminated patches") are saved for field analysis. By so doing, a considerable amount in CPU time and computer memory can be saved. At this stage, these patches will be selected considering only those that are simultaneously seen by the source point and the observation point or observation direction, depending on whether the receiver antenna is considered in the near or far field, respectively. This selection criterium is used because from authors experience, the contribution from the nonselected patches is nearly negligible, except for the creeping mechanism where all the patches should be considered.

In the third step of the approach, the field levels are computed. The following field contributions have been considered: 1) direct field from the source; 2) reflected fields from the BP's of the model; 3) diffracted fields from the arbitrary edges defined as Bèzier curves (BC); 4) double-reflected field; and 5) diffracted–reflected and reflected–diffracted fields. The ray-tracing algorithm is the opposite to the shooting and bouncing technique—given an observation direction, calculate all the rays that contribute to that direction. For all these field contributions, a set of fast criteria is applied to each one of the previously selected BP's to determine whether this BP has any chance of being involved in this field contribution. These criteria eliminate very efficiently practically all the BP's from being studied in more detail. Only the patches that fulfill these criteria are examined in detail if the ray path is interrupted by the structure.

In the fourth step, the contribution from the creeping waves is computed. For this purpose, a new remeshing of the model is performed automatically, taking into consideration all the BP's of the model. This remeshing is also based on the BP, but now, the geodesic lines followed by the creeping waves coincide with the parametric lines of one of the coordinates of the new BP. Using this remeshing, it is now quite easy to solve the inverse problem: given a far-field direction or a near-field point, find out if a connection with the source by a creeping wave exists and, eventually, obtain its corresponding path. The description of this part of the approach, where the creeping waves are evaluated, will be treated in another paper.

This paper is organized as follows. Section II presents the geometrical modeling and the method developed to select the illuminated BP. Section III shows the technique used to find the reflection and diffraction points and the calculations of the fields due to the different effects considered. Section IV presents results for the validation of the approach. Finally, Section V outlines the conclusions.

II. Geometrical Model Definition and Preprocessing

Two parts will be considered in this section. In a first moment, a summary of the main properties of NURBS and Bèzier patches is briefly presented. The second part outlines the preprocessing of the geometry to improve the efficiency of the proposed approach.

A. Modeling by NURBS and Bèzier Patches

A NURBS surface is a rational piecewise parametric surface defined by an array of control points, their associated weights, and two knot vectors [7], [17]. Surface points coordinates are given in terms of polynomials of the parameters u and v. Flat patches (triangle, polygonal plates) and conic sections are particular types of NURBS. Some properties about these surfaces can be found in [7] and [15]–[17]. An arbitrary structure is modeled by a collection of individual NURBS patches providing the complete description of its surface. The model can be easily obtained from many of the CAGD tools. An example of a NURBS model is shown in Fig. 1(a).

NURBS surfaces can be easily transformed into BP's applying the Cox-De Boor algorithm [18]. The number of BP's obtained from a NURBS surface depends on its knot vector numbers. A BP is also a parametric surface defined in terms of a linear combination of Bernstein's polynomials. The Bèzier format is numerically more stable for rendering surface parameters than the B-spline form thanks to the characteristics of Bernstein's basis. This feature means that the Bèzier form is suitable for the numerical computation of parameters associated with the geometry such as curvatures, derivatives, etc. Surface points coordinates and their parametric derivatives are given also in terms of linear combinations of Bernstein's polynomials that can be easily computed [7], [15], [17].

The analysis of the edges in a NURBS model is quite straightforward. From the study of the normal discontinuities at the boundary curves between NURBS it is possible to decide which boundary curve must be considered as an edge for diffraction effects. The B-spline curve that defines the union between NURBS surfaces is divided into BC following the same process as for surfaces.

The initial description of the model by NURBS surfaces will be accompanied by other complementary geometric data—the topology of the surfaces, boundary curves, the type of material, the shape of the patch, etc. In addition, most CAGD tools provide NURBS surfaces arranged in blocks, each block

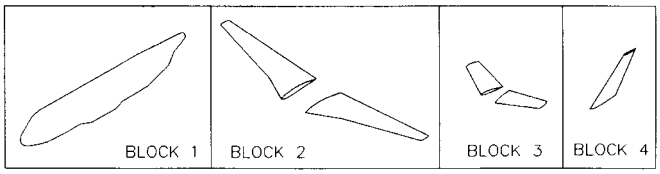

Fig. 2. Example of the development of an aircraft model in terms of blocks.

representing a different part of the model. Fig. 2 shows an example of an arrangement by blocks of an aircraft. This arrangement simplifies the analysis of bodies especially when interactions among surfaces are studied.

In summary, NURBS geometry is expanded in terms of a collection of BP's and BC's forming a wedge-surface model where the GO-UTD theory is directly applied. More information about parametric representation of structures can be found in [19]–[21].

B. Geometrical Preprocessing

The preprocessing starts with the selection of the geometry illuminated by the source. It must be remembered that the philosophy behind the ray analysis process is to discard, at the earliest opportunity, the part of the geometry that does not contribute to the scattering effects. Although NURBS format is preferred for storage due to data compression, for illuminating selection criteria, it is better to work with smaller surfaces to eliminate the major part of the body. Therefore, only the BP and BC illuminated from the source will be considered during the analysis.

To apply the selection criteria, two sets of vectors associated with each BP or each BC must be considered; these vectors are shown in Fig. 3. Vectors *Ni* in Fig. 3(a) are normal to the surface at nine sample points *Pi* regularly distributed over the parametric space of the BP. The *FPi* vectors in Fig. 3(b) represent the vectors that join the source at $\bar{F}$ with the sample points *Pi*, and they will be called "enveloping vectors." In the BC case, Fig. 3(c), vectors *N1-i* and *N2-i* are normal to surfaces *B1* and *B2* at sample points *P*i on the BC. *FPi* vectors in Fig. 3(d) join the source at *F* with the points *Pi*. Finally, *Ti's* in this figure are the tangent vectors to the BC at the sample points.

The illuminated selection criterium is based on the back-face culling algorithm—the BP or BC susceptible to be illuminated are identified by the nonnegative dot product between their vectors *Ni* and *FPi* [22], [23].

The BP's that support the antenna will be known as "antenna patches" and an example of an antenna patch is shown in Fig. 4. The treatment of these patches should take priority because they are exposed to the greatest radiated field by the source and usually represent the main contribution to the scattered field. On the other hand, antenna patches lie very near the source and consequently project large shadow regions over the rest of the model. The BP and BC previously detected as illuminated are analyzed to find out if they are shadowed by antenna patches. At the end of the selection and hiding process, the geometry data to be stored is considerably smaller than the initial description of the body, as Fig. 1(b) shows.

III. Field Computations

This part starts with a description of the antenna model considered, followed by the analysis of the coupling mechanisms due to direct ray, reflected ray, diffracted ray, and double effects.

A. Electromagnetic Modeling of the Antenna

Most airborne antennas operate above 100 MHz and they are mounted on electrically large platforms, therefore, a high-frequency approach is appropriate. In our method, the antennas are electrically modeled by the superposition of GO fields radiated by a small set of infinitesimal electric and magnetic dipoles. These sets are obtained by imposing that the far-field radiated patterns of the dipoles set are similar to the measured radiated patterns of the antennas when they are mounted on electrically large platforms such as circular ground planes [24]. It has been shown that these antenna models are practically invariable with changes in the geometry of the supporting structure, thus, it is very advantageous for engineering applications. Another possibility is to represent the antenna by several cuts of its radiation pattern. In this last case, interpolation techniques shall be used to obtain the field in arbitrary directions.

B. Direct-Field Computation

The direct field is calculated by applying the principle of superposition to all the dipoles that compose the antenna electrical model. The GO expressions will be applied to obtain both the far-field and near-field cases [25]–[29].

To analyze whether a direct field is shadowed by the structure, only the BP's previously selected as illuminated are used. The patches of this set are analyzed one by one until a BP (if any) is found intersecting the ray path. At this moment, the shadow study for this ray ends. All the illuminated patches shall be considered by the shadowing study although only very few of them, if any, will intersect the ray path. So when a ray path is studied, first we need to employ fast criteria that will help us to classify quickly most of the illuminated BP as not "shadower." Only very few potential shadower BP's will pass these criteria. A rigorous intersection algorithm will be applied only to these last BP's.

The fast criteria are based on the application of the dot product between the incident direction and each of the enveloping vectors corresponding to the BP at the sample points. Two fast criteria have been considered in the shadowing analysis: back-face culling and the boundary-boxes algorithm [30]. First, the back-face culling algorithm is applied to the sample points *Pi* associated with each one of the enveloping vectors of the BP under analysis. If the BP passes the above criterium for all the sample points, the boundary-boxes algorithm is applied. This last criterium lies in the study of the intersection of the incident ray with the box that enclosed the BP. This bounding box is easily obtained from the control points of the BP. If there is no intersection with the box, there is no intersection with the BP.

The intersection point is calculated rigorously by applying the conjugate gradient method (CGM) [31]. This method is

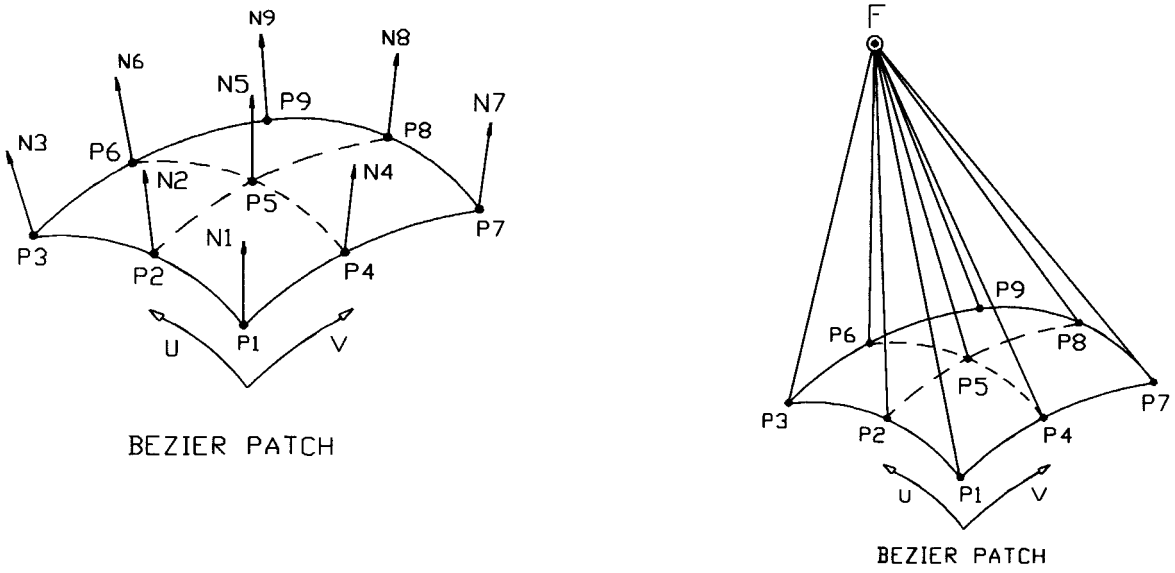

Fig. 3. Vectors associated with BP and BC.

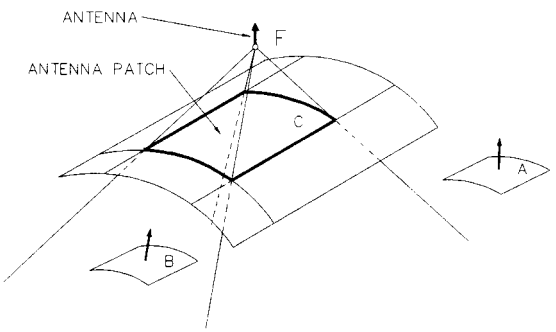

Fig. 4. Example of an antenna patch. BP's A and B are given as illuminated using the back-face culling algorithm. However, the BP is shadowed by the antenna patch and, therefore, it shall not be considered in the analysis of an antenna that has its focus on F.

used to find the minimum of the function that gives the distance between the points of the BP and the straight line defined by the direct ray. The distance is a function of the parametric coordinates of the point on the BP under analysis. The problem is illustrated in Fig. 5, where *VI* is the ray direction, $P(u,v)$ is the point of the parametric surface defined by u and v, and D is the distance between the point P and the ray path. The parametric coordinates of the solution point must lie on the interval [0, 1] for both u and v.

C. Reflected-Field Computation

To compute the reflection points on the geometry it is necessary to take into account the observation direction and the incident direction on the surface. The back-face culling and the boundary-boxes algorithms are used as fast criteria. The first is applied considering both the incident and the observation ray directions. Once a BP survives the eliminating criteria, then the rigorous reflection algorithm will be applied.

The problem is shown in Fig. 6, where VI is the incident direction, VR the reflection direction, $P(u,v)$ is a point on the BP, $S(u,v)$ is the BP surface, *D1* is the distance between the

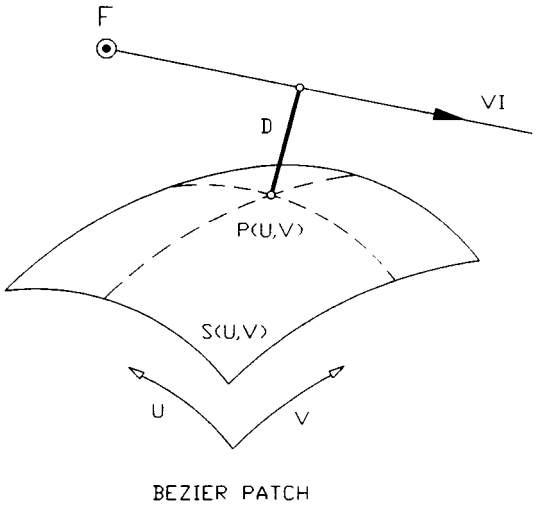

Fig. 5. Treatment of the ray intersection problem.

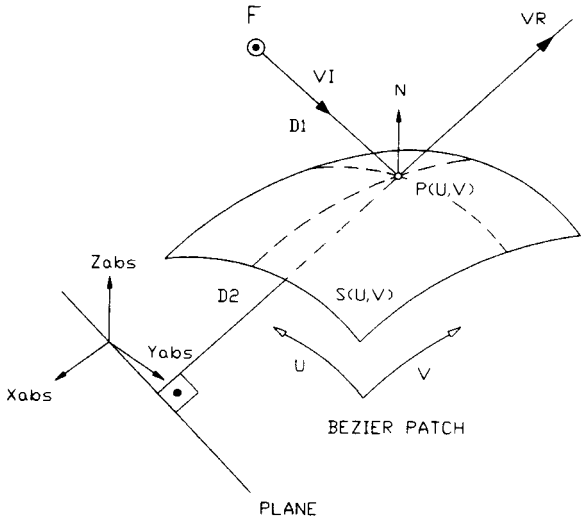

Fig. 6. Treatment of the ray reflection problem.

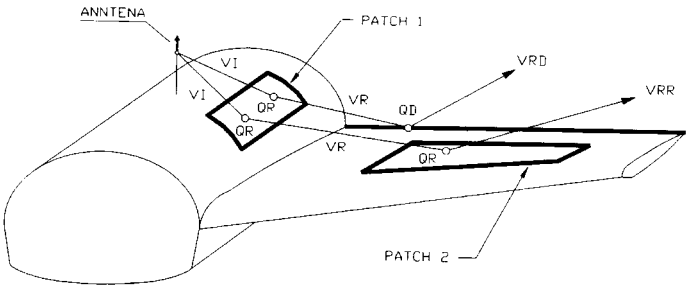

Fig. 7. Double reflection and reflection–diffraction between two different blocks.

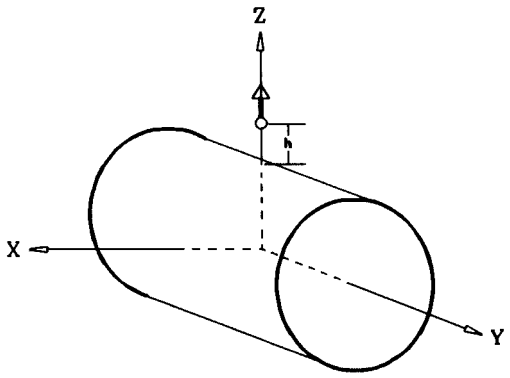

(a)

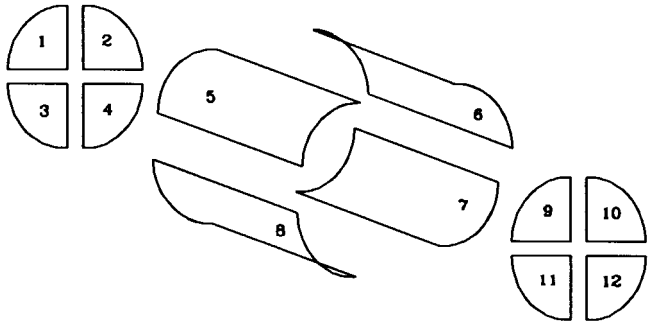

(b)

Fig. 8. Cylinder modeled with 12 NURBS surfaces. Radius $= 0.25$ m. Length $= 1$ m, $h = 0.25$ m.

point P and the antenna location denoted by F, and *D2* is the distance between the point P and a plane perpendicular to VR which cuts the origin of the absolute coordinates system. In the near-field case, the distance *D2* is replaced by the distance between P and the test point of the near field. The rigorous algorithm used to check if there is a reflection point and eventually find this point, is based on the conjugate gradient (CG) method. The algorithm minimizes a function defined by the sum of the two distances, *D1* and *D2*. The minimization procedure is based on the Fermat principle.

Once the reflection point $Q_r(u,v)$ has been found, the reflection dyadic $\overline{\overline{R}}$ can be calculated easily [32], [33]. The dyadic expression $\overline{\overline{R}}$ in terms of their corresponding soft and hard functions is defined as

$$\overline{\overline{R}} = R_s \hat{e}_{\perp}\hat{e}_{\perp} + R_h \hat{e}_{\parallel}\hat{e}_{\parallel} \tag{1}$$

where the coefficients R_s and R_h are defined in detail in [32]. To compute these coefficients it is necessary to know geometrical parameters like the normal vector and the surface radius of curvature ρ_g in the direction of the reflected ray. These parameters are directly calculated from the geometric description of the BP [7]. At this point it is interesting to note that we are using the classic GO/UTD, which cannot be used to calculate scattered field from concave–convex surfaces. Due to this limitation, in our approach, patches with concave shape are not allowed in the structure description. In cases where such geometries should be of importance, the above restriction can be overcome implementing the UGO/EUTD solution presented in [34] which enables the scattered field from concave–convex surfaces to be analyzed.

D. Diffracted-Field Computation

Similar the reflected field-computation with boundary-boxes and back-face culling techniques are used as fast criteria. However, in this case, a BC is involved and two normal vectors, the sampling points, must be taken into account in this application of the back-face culling criterium. As in the

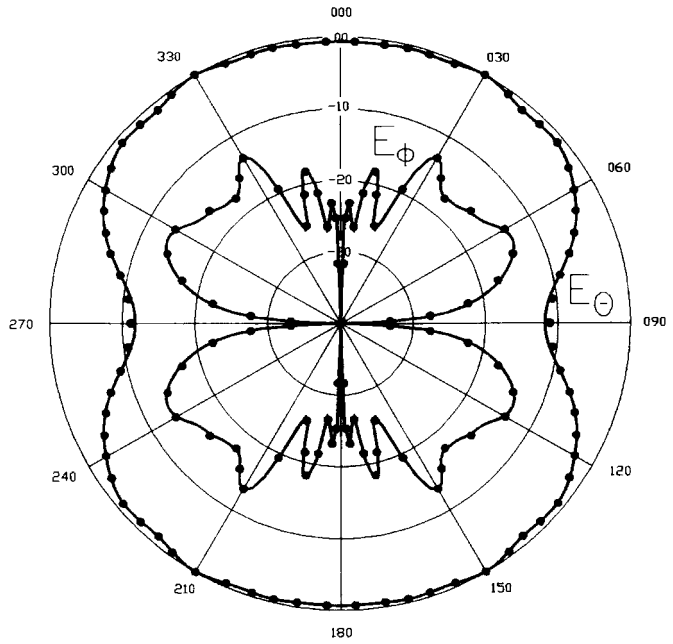

Fig. 9. E_θ and E_ϕ components for azimuth conical pattern $\theta = 45°$ for the cylinder case. Frequency = 3 GHz: NEC/BSC (dotted line) and our approach (continuous line).

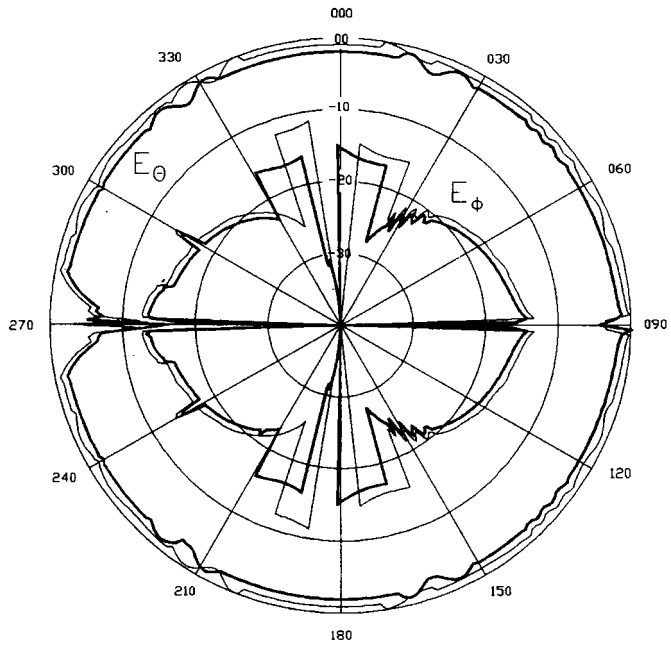

Fig. 11. E_θ and E_ϕ components for the cut $\theta = 90°$ for the simplified aircraft case: NEC/BSC (thin line) and our approach (thick line).

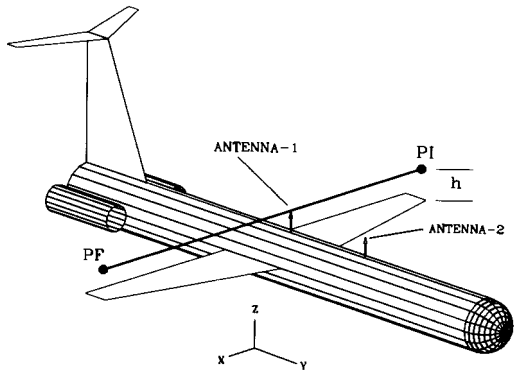

Fig. 10. Simplified model of an aircraft. An electrical dipole is located at point ANTENNA-1 for the far-field case and ANTENNA-2 for the near-field case, oriented perpendicularly to the main cylinder that represents the aircraft fuselage. The distance between the monopole and the cylinder is 0.05 m. The continuous line PI-PF contains the points considered for near-field computation.

reflected field computation, the rigorous method is also based on the CGM that is only applied to the BC which survived to the fast criteria. In this case, the distance function only depends on the parametric coordinate of the BC.

Once the diffraction point $Q_e(u)$ has been found, the UTD expression can be applied easily [33]. The dyadic expression $\overline{\overline{D}}$ in terms of their corresponding acoustic soft and hard functions is defined as

$$\overline{\overline{D}} = -D_s\hat{\beta}_o'\hat{\beta}_o - D_h\hat{\phi}'\hat{\phi} \tag{2}$$

where the coefficients D_s and D_h are defined in detail in [33]. The coefficients depend on the unit vectors $\vec{n}_o$ and $\vec{n}_n$ that are normal to the pair of BP which define the edge, the radius of curvature of the edge a_e at Q_e, the vector tangent to the edge $\vec{e}$ at Q_e, and the vector normal to the edge at $Q_e, \vec{n}_e$. The radius of curvature a_e and the vectors $\vec{e}$ and $\vec{n}_e$ can be obtained directly from the BC that defines the edge [7].

A limitation of the method is the probability (very low) of coalescence of diffraction points creating caustics.

E. Double-Effects Computations

In this approach, the following second-order effects have been considered: double-reflection (RR), reflection–diffraction (RD), and diffraction–reflection (DR). Simple GO and UTD are used for the reflections and the diffractions, respectively. Usually, the above effects are the most important field contributors among the second-order coupling mechanisms. In fact, due to the antenna pattern effects, RR, RD, and DR can give field values greater than a direct ray.

From a computational point of view, the inclusion of double effects is quite a cumbersome task. In addition, the CPU time required for the evaluation of a double effect is considerable greater than that needed to compute a simple effect. Therefore, the implementation in a computer code of double effects requires special care.

As in first-order effects, only BP's and BC's directly illuminated are taken into account in the ray-tracing analysis. With this strategy, memory requirements and CPU time are meaningfully reduced. In some particular situations, BP's from the shadow regions could be involved in the ray-tracing and, shadowed, the method fails. But these cases have a low probability of happening.

In the strategy to find the ray paths for double effects an additional fast criterium is applied. It is based on the fact that it is nearly impossible that double effects could appear among the patches of the same block of the body. Examining the blocks of the aircraft (Fig. 2), we can assess this phenomenon. Usually, most of the computer-aided geometric design (CAGD) tools provide a block division of the bodies under analysis.

Moreover, a set of fast eliminating criteria, which are a generalization of those outlined for the simple reflection and diffraction, is used. Finally, the Fermat principle in combination with the CGM is used to find the ray paths (see Fig. 7).

Once the ray paths have been found, the contribution of a RR, RD, or DR mechanism can be expressed in terms of the parameters that define the BP or BC where the reflection or diffraction points are located.

IV. Results

The results of three cases are given to illustrate how useful this approach is for predicting the radiation patterns and near-field values of antennas on board arbitrary structures modeled by NURBS surfaces. In the first problem, a very simple structure (a cylinder) has been considered. In the second problem, a simplified model of an aircraft composed of a few cylinders and plane facets is analyzed. Finally, in the third case, a cylinder-plate model is presented. The results are compared to the moment-method solution, taking into account the double-effects contribution. In the cases of the cylinder and the simplified aircraft, our results are compared with computed values obtained using the code numerical electromagnetic code/basic scattering code (NEC/BSC) [35]. Our approach and NEC/BSC use basically the same UTD expressions, but the former can analyze arbitrarily curved surfaces, whereas the latter is restricted to flat plates, cylinders, and probably some spheroids surfaces in most recent versions. For most researchers, NEC/BSC is a very reliable code that can be employed for validation purposes.

A. Cylinder

The cylinder shown in Fig. 8 is the first example to demonstrate the agreement between a code based in the present approach and NEC/BSC. The cylinder is modeled with 12 NURBS patches, as indicated in Fig. 8(b). Each one of them generates only one BP. The example considers an electric dipole perpendicular to the cylinder and located, as shown in Fig. 8(a). Fig. 9 presents a comparison between results using NEC/BSC and our code for the E_θ and E_ϕ components in a conical cut of the radiation pattern. Only direct, reflected, and diffracted fields are considered in the results. A high level of agreement between the results of both codes can be appreciated.

B. Simplified Model of an Aircraft

A simplified model of an aircraft together with the antenna location is pictured in Fig. 10. The main dimensions of the aircraft are 21-m length and 7-m height and it has a 16-m wingspan. Again, a comparison between results obtained at 3 GHz using NEC/BSC and our code is possible because the model is composed of plane plates and circular cylinders, such as is required by the NEC/BSC. Only direct, reflected, and diffracted rays have been considered because our NEC/BSC version cannot manage with double effects on cylinders. In our approach, the model is represented by 26 NURBS patches that generate the same number of BP's. Results for the E_θ and E_ϕ components are shown in Fig. 11. The agreement between the results of both codes seems reasonably good.

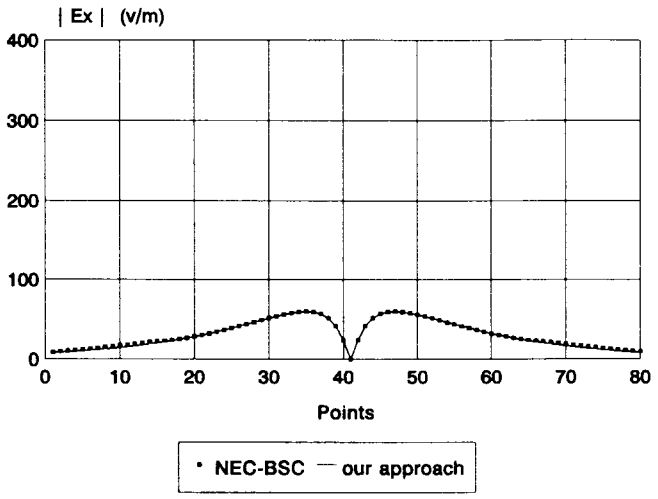

(a)

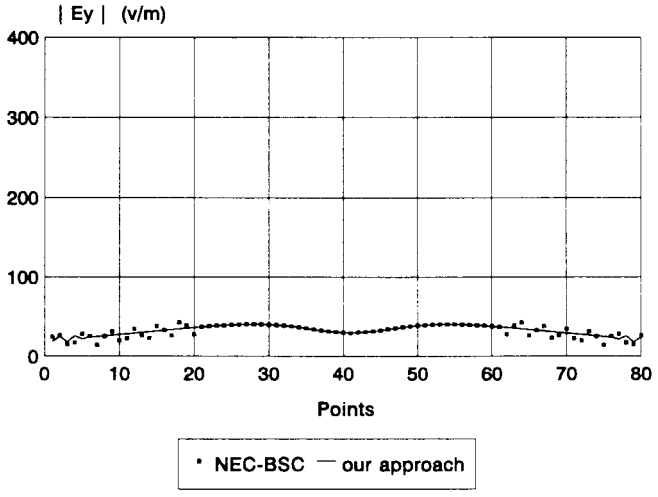

(b)

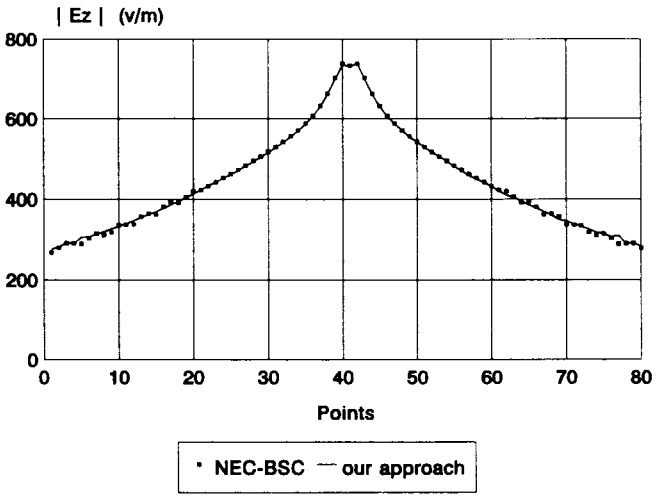

(c)

Fig. 12. (a) E_x component along the PI-PF line indicated in Fig. 10. (b) E_y component along PI-PF line. (c) E_z component along PI-PF line.

To obtain an idea of the behavior of our approach in computing near-field values, a set of points, regularly spaced

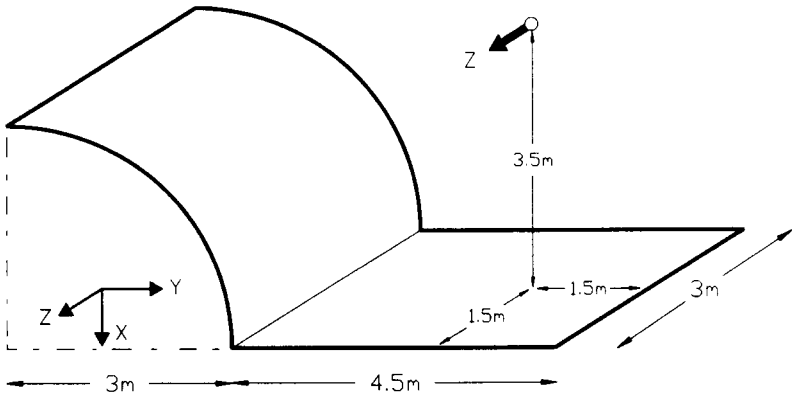

Fig. 13. Cylinder-plate geometry.

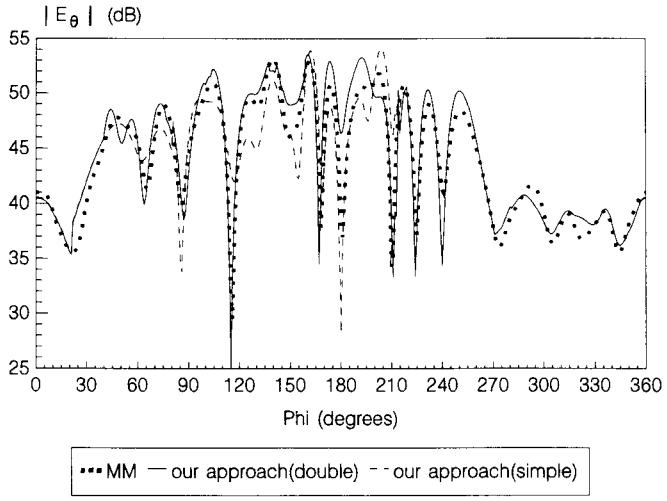

Fig. 14. Cylinder-plate results compared with MoM for cut $\theta = 90°$.

along the line PI-PF of Fig. 10, has been considered. This line is parallel to the aircraft wings. The distance between the line and the wing h is 1.2 m. Fig. 12 shows the three Cartesian components of the near-electric field along the line PI-PF using NEC/BSC and our code. The field source is the dipole ANTENNA-2 of Fig. 10 working at 3 GHz. The number of points considered for near-field computation was 80. Once again, only the coupling mechanisms generated by direct ray, reflected ray, and diffracted rays have been taken into account to make a coherent comparison between the results obtained with both codes. Examining Fig. 12, an almost complete agreement between the results of both codes is evident.

C. Cylinder Plate

Fig. 13 shows the analyzed geometry where double effects seem to have a great importance. The geometry, modeled by two NURBS surfaces, consists of a square plate of dimensions $3\lambda \times 4.5\lambda$ and a quarter section of a cylinder with a 3λ radius. The frequency of analysis is 0.3 GHz. The antenna is an infinitesimal electric dipole oriented along z axis. Fig. 14 shows the cut $\theta = 90°$ and displays three different solutions: our approach-total field only with simple effects (dashed line), our approach-total field including simple and double effects (continuous line), and the MM solution (dotted line). The last curve has been obtained with the code resulting from [17].

Regarding this result, the improvement that the double effects represent in the angular margin, which range approximately from $\phi = 60°$ to $\phi = 180°$, has to be mentioned. These results can be considered good enough if the electric size of the geometry is taken into account—too small for high-frequency methods. At this frequency, other second-order effects such as corner diffraction, diffraction-diffraction, etc. could be important. These effects will be irrelevant when the electric size of the geometry increases.

V. Conclusion

The approach presented in this paper combines the UTD with parametric curves and surfaces to predict the antenna radiation patterns on board arbitrary three-dimensional objects. The significance of this approach is that NURBS surfaces are able to manipulate both free-form surfaces and primitive quadric surfaces (cylinders, spheres, etc.) with a low number of patches. These advantages of the parametric surfaces simplify the applications of high-frequency techniques. Radiation patterns for several cases have been analyzed successfully. With this new treatment of the problem, arbitrary and complex geometries (satellites, airplanes, cars, ships, etc.) can be analyzed using very little CPU time. The numerical solution obtained can be used to examine quickly several antenna configurations in the top-side design stage of a craft employing the same geometrical model as in other engineering areas (mechanical, structural, aerodynamic, etc.).

References

[1] W. D. Burnside, M. C. Gilreath, R. J. Marhefka, and C .L. Yu, "A study of KC-135 aircraft antenna patterns," *IEEE Trans. Antennas Propagat.*, vol. AP-23, pp. 309–316, May 1975.

[2] C. L. Yu, W. D. Burnside, and M. C. Gilreath, "Volumetric pattern analysis of airborne antennas," *IEEE Trans. Antennas Propagat.*, vol. AP-26, pp. 636–641, Sept. 1978.

[3] W. D. Burnside, N. Wang, and E. L. Pelton, "Near-field pattern analysis of airborne antennas," *IEEE Trans. Antennas Propagat.*, vol. AP-28, pp. 318–327, May 1980.

[4] J. J. Kim and W. D. Burnside, "Simulation and analysis of antennas radiating in a complex environment," *IEEE Trans. Antennas Propagat.*, vol. AP-34, pp. 554–562, Apr. 1986.

[5] W. D. Burnside and R. J. Marhefka, "Antennas on aircraft, ships or any large complex environment," in *Antenna Handbook: Theory, Applications, and Design*, Y. T. Lo and S. W. Lee, Eds. New York: Van Nostrand Reinhold, 1988, ch. 20.

[6] R. J. Marhefka and W. D. Burnside, "Antennas on complex platforms," *Proc. IEEE*, vol. 80, pp. 204–208, Jan. 1992.
[7] G. Farin, *Curves and Surfaces for Computer-Aided Geometric Design*. New York: Academic, 1988.
[8] M. I. Sancer, R. L. McClary, and K. J. Gover, "Electromagnetic computation using parametric geometry," *Electromagn.*, vol. 10, pp. 85–103, Jan.-Mar. 1990.
[9] J. Pérez and M. F. Cátedra, "RCS of electrically large targets modeled with NURBS surfaces," *Electron. Lett.*, vol. 28, no. 12, pp. 1119–1121, June 1992.
[10] ——, "RCS of targets modeled with NURBS surfaces," in *IEEE Antennas Propagat. Int. Symp.*, Chicago, IL, July 1992, vol. 2, pp. 965–968.
[11] T. A. Blalock. "Modern RCS computations—A practical approach," in *IEEE Antennas Propagat. Int. Symp.*, Chicago, IL, July 1992, vol. 3, pp. 1298–1301.
[12] D. M. Elking, S. D. Alspach, D. D. Car, K. E. Castle, J. L. Karty, J. H. Knebans, R. A. Perlman, and J. M. Roedder, "Electromagnetic Analysis Codes," in *IEEE Antennas Propagat. Int. Symp.*, Chicago, IL, July 1992, vol. 3, pp. 1306–1309.
[13] A. García-Pino, F. Obelleiro, J. L. Rodríguez, and A. M. Arias, "A comparison of ray-tracing methods for the analysis of high frequency scattering by arbitrary shaped cavities," in *URSI Radio Sci. Meet.*, Chicago, IL, July 1992, vol. 1, p. 505.
[14] J. M. Rius, M. Ferrando, and L. Jofre, "GRECO: Graphical electromagnetic computing for RCS prediction in real time," *IEEE Antennas Propagat. Mag.*, vol. 35, pp. 7–17, Apr. 1993.
[15] J. Pérez and M. F. Cátedra, "Application of physical optics to the RCS computation of bodies modeled with NURBS surfaces," *IEEE Trans. Antennas Propagat.*, vol. 42, pp. 1404–1411, Oct. 1994.
[16] M. Domingo, F. Rivas, J. Pérez, R. P. Torres, and M. F. Cátedra, "Computation of the RCS of complex bodies modeled using NURBS surfaces," *IEEE Antennas Propagat. Mag.*, vol. 37, pp. 36–47, Dec. 1995.
[17] L. Valle, F. Rivas and M. F. Cátedra, "Combining the moment method with geometrical modeling by NURBS surfaces and Bèzier patches," *IEEE Trans. Antennas Propagat.*, vol. 42, pp. 373–381, Mar. 1994.
[18] W. Boehm, "Generating the Bèzier points of B-spline curves and surfaces," *Comput.-Aided Design*, vol. 13, no. 16, pp. 365–366, 1981.
[19] M. E. Mortenson, *Geometric Modeling*. New York: Wiley, 1985.
[20] W. Tiller, "Rational B-splines for curve and surface representation," *IEEE Comput. Graphics Applicat.*, vol. 3, pp. 61–69, Sept. 1983.
[21] R. E. Barnhill and R. F. Riesenfeld, *Computer-Aided Geometric Design*. New York: Academic, 1974.
[22] J. D. Foley, A. Van Dam, S. K. Feiner, and J. F. Hughes, *Computer Graphics, Principles, and Practice*. Reading, MA: Addison-Wesley, 1990.
[23] David F. Rogers, *Procedural Elements for Computer Graphics*. New York: McGraw-Hill, 1985.
[24] M. Domingo, P. Martínez, and R. P. Torres, "Simple numerical models for on board antennas," in *PIERS Progress Electromagn. Res. Symp.*, Noordwijk, The Netherlands, July 1994, pp. 1665–1668.
[25] C. A. Balanis, *Antenna Theory, Analysis and Design*. New York: Wiley, 1982.
[26] ——, *Advanced Engineering Electromagnetics*. New York: Wiley, 1989.
[27] R. H. Clarke and J. Brown, *Diffraction Theory and Antennas*. New York: Wiley, 1980.
[28] D. A. McNamara, C. W. I. Pistorius, and J. A. G. Malherbe, *Introduction to the Uniform Geometrical Theory of Diffraction*. Norwood, MA: Artech, 1990.
[29] G. L. James, *Geometrical Theory of Diffraction for Electromagnetic Waves*. London, U.K.: Inst. Elect. Eng. Electromagn. Waves, 1986, ser. 1.
[30] Chang-Gui Yang, "On speeding up ray tracing of B-spline surfaces," *Comput.-Aided Design*, vol. 19, no. 3, pp. 122–130, Apr. 1987.
[31] W. H. Press, B. P. Flannery, S. A. Teukolsky, and W. T. Vetterling, *Numerical Recipes*. Cambridge, U.K.: Cambridge Univ. Press, 1987.
[32] P. H. Pathak, W. D. Burnside, and R. J. Marhefka, "A uniform GTD analysis of the diffraction of electromagnetic waves by a smooth convex surface," *IEEE Trans. Antennas Propagat.*, vol. AP-28, pp. 631–642, Sept. 1980.
[33] R. G. Kouyoumjiam and P. H. Pathak. "A uniform geometrical theory of diffraction for an edge in a perfectly conducting surface," *Proc. IEEE*, vol. 62, pp. 1448–1461, Nov. 1974.
[34] E. D. Constantinides and R. J. Marhefka. "A UGO/EUTD solution for the scattering and diffraction from cubic polynomial strips," *IEEE Trans. Antennas Propagat.*, vol. 41, pp. 1088–1098, Aug. 1993.
[35] R. J. Marhefka and W. D. Burnside, "Numerical electromagnetic code-basic scattering code NEC-BSC (V2)," Tech. Rep., ElectroSci. Lab., The Ohio State Univ., Dec. 1982.

Jesús Pérez (S'93), for photograph and biography, see p. 1411 of the October 1994 issue of this TRANSACTIONS.

Juan A. Saiz (S'93) was born in Santander, Spain. He received the B.Sc. (in physics) and Ph.D. degrees from the University of Cantabria, Spain, in 1990 and 1995, respectively.

He is an Associate Professor of electromagnetics at the University of Cantabria, Spain, and has been with the Communications Engineering Department there since 1990, where he is working in the areas of numerical analysis of electromagnetic radiation and scattering problems.

Olga M. Conde (S'95) was born in Torrelavega, Spain, in 1970. She received the B.Sc. degree in telecommunications engineering from the University of Cantabria, Spain, in 1994. She is currently working toward the Ph.D. degree at the same university.

Since 1993, she has been with the Communications Engineering Department, University of Cantabria. Her research interests include electromagnetic scattering and propagation on complex structures and cellular environments.

Rafael P. Torres (M'91) was born in Málaga, Spain, in 1961. He received the M.S. degree in physics from the University of Granada, Spain, and the Ph.D. degree in telecommunications engineering from the Polytechnic University of Madrid (UPM), Spain, in 1986 and 1990, respectively.

From 1986 to 1990, he was with the Radio Communication and Signal Processing Department of UPM as a Research Assistant. During this time, he worked on numerical methods in electromagnetics and their applications to the design of passive microwave devices such as radomes, circular polarizer, rotator and planar lenses. He became an Associate Professor in the Electronic Department of the University of Cantabria, Spain, in 1990. From 1990 to the present he has participated in several projects involving RCS computation, on-board antennas analysis, and electromagnetic compatibility. He is co-author of a book about the CG-FFT method, several chapters in different books and papers, and about 40 conference contributions. His research interests include numerical and high-frequency methods in electromagnetics applied to antennas and microwave components, radio-propagation, and mobile communications.

Manuel F. Cátedra (S'80–M'82), for photograph and biography, see p. 213 of the February 1993 issue of this TRANSACTIONS.